Optics Letters

Temperature-insensitive curvature sensor based on Bragg gratings written in strongly coupled multicore fiber

Zhiming Liu,[1] Di Zheng,[1,*] Javier Madrigal,[2] Joel Villatoro,[3,4] J. Enrique Antonio-Lopez,[5] Axel Schülzgen,[5] Rodrigo Amezcua-Correa,[5] Xihua Zou,[1] Wei Pan,[1] and Salvador Sales[2]

[1]Center for Information Photonics & Communications, School of Information Science & Technology, Southwest Jiaotong University, Chengdu 610031, China
[2]Photonics Research Labs, ITEAM Research Institute, Universitat Politècnica de València, Camino de Vera, s/n, 46022 Valencia, Spain
[3]Department of Communications Engineering, University of the Basque Country UPV/EHU, Plaza Torres Quevedo 1, E 48013 Bilbao, Spain
[4]IKERBASQUE–Basque Foundation for Science, Bilbao E 48011, Spain
[5]University of Central Florida, CREOL, The College of Optics and Photonics, Orlando, Florida 32816, USA
*Corresponding author: dzheng@home.swjtu.edu.cn

Received 11 June 2021; accepted 5 July 2021; posted 8 July 2021 (Doc. ID 432889); published 9 August 2021

A novel temperature-insensitive optical curvature sensor has been proposed and demonstrated. The sensor is fabricated by inscribing fiber Bragg gratings with short lengths into a piece of strongly coupled multicore fiber (SCMCF) and spliced to the conventional single-mode fiber. Due to the two supermodes being supported by the SCMCF, two resonance peaks, along with a deep notch between them, were observed in the reflection spectrum. The experimental results show that the depth of the notch changes with the curvature with a sensitivity up to 15.9 dB/m^{-1} in a lower curvature range. Besides, thanks to the unique property of the proposed sensor, the notch depth barely changes with temperature. Based on the intensity demodulation of the notch depth, the temperature-insensitive curvature sensor is achieved with the cross sensitivity between the temperature, and the curvature is as low as 0.001 m^{-1}/°C.

https://doi.org/10.1364/OL.432889

Compared to conventional electric sensors, optical fiber sensors have unique advantages such as high sensitivity, light weight, and immunity to electromagnetic interference. All these favorable aspects make optical fiber sensors attractive for measuring different parameters such as the refractive index [1], transverse load [2], strain [3], and curvature [4]. In the past few decades, numerous advanced fiber optics sensors have been manufactured with the emergence of new types of specialty optical fibers. In particular, the enormous potential of multicore fiber (MCF) in plentiful applications such as broadband communications, microwave photonics, and optical sensing [5–7], has attracted extensive attention. The superior characteristics of the MCF provide new options for the development of innovative devices with performance and functionalities that cannot be easily achieved with traditional single core fiber. In particular, in the field of optical fiber sensing, many research groups have reported the use of MCFs to construct different sensors to measure various measurands, including the shape [8], curvature [9], strain [10], refractive index, and temperature [11]. So far, most of the reported MCF-based sensors are built with weakly coupled MCFs in which each core acts as a separate waveguide with negligible mode coupling among adjacent cores. For these MCFs, it is unavoidable to use expensive fan-in/out devices to interrogate each individual core of the fiber, which increases the complexity and cost of the interrogation system.

In recent years, a new type of MCF, called strongly coupled multicore fiber (SCMCF), has drawn considerable research interest. In a SCMCF, specific supermodes can be excited, depending on the excitation conditions; each supermode can be regarded as one spatial channel [12]. One of the significant advantages of SCMCF-based sensors is that their interrogation is very simple; it can be carried out with a standard single-mode fiber (SMF) fusion spliced to the SCMCF. Therefore, the interrogation system of SCMCF-based sensors can be done with widely available equipment. In our previous works, SCMCFs have been designed as a variety of interferometric sensors for different measurands such as temperature [13], strain [14], or bend [15]. These SCMCF-based sensors exhibit excellent performance in terms of sensitivity and accuracy. In addition, the fabrication of the SCMCF sensor is straightforward and reproducible, making it an inexpensive fiber device.

In this Letter, the combination of SCMCFs and fiber Bragg grating (FBGs) is proposed to create a temperature-insensitive optical curvature sensor for the first time, to the best of our knowledge. Due to the unique characteristic of the SCMCF that supports specific supermodes, the reflection spectrum of the FBG inscribed in the SCMCF generates a deep notch between two neighboring Bragg wavelengths. In particular, the depth of notch changes with the curvature, while it is insensitive to temperature. Therefore, by intensity demodulation of the notch depth, a temperature-insensitive curvature sensor was achieved.

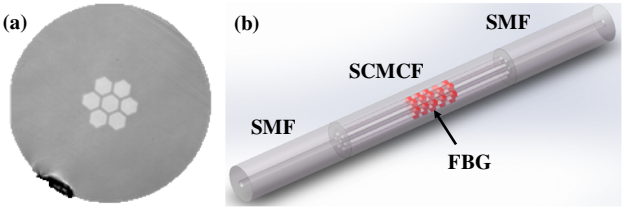

Fig. 1. (a) Micrograph of the cross section of the SCMCF. (b) Schematic structure of the proposed sensor.

The experimental results demonstrated that the curvature sensitivity is up to 15.9 dB/m^{-1} within a range from 0 to 0.7 m^{-1} and is insensitive to bending direction. The temperature-curvature cross sensitivity is less than 0.001 m^{-1}/°C. The proposed curvature sensor has the advantages of a compact structure, easy interrogation, and low cross-sensitivity.

The SCMCF used to design our sensor was fabricated at the facilities of the University of Central Florida (Orlando, USA). A micrograph of the cross section of the fiber is shown in Fig. 1(a). The SCMCF consists of seven identical cores arranged in a regular hexagon with a core separation of 11 μm. The diameter of each core is 9.2 μm. The numerical aperture of each core is designed to match that of a conventional SMF. Thus, coupling loss is minimized when our SCMCF is spliced to the SMF. The schematic structure of the proposed sensor is shown in Fig. 1(b). To inscribe FBGs in the SCMCF, first, it is hydrogen loaded at ambient temperature for two weeks at a pressure of 50 bar. Then the UV phase mask technique is used to inscribe the gratings into the SCMCF. Finally, for convenience of characterizing the reflection spectrum of FBGs with a commercial optical spectrum analyzer, a section of SMF is fusion spliced to the end of the SCMCF. The SMF–SCMCF junctions were produced with a conventional fusion splicer (Fujikura FSM-45PM). The machine was configured to use the multimode fiber splicing program with a fusion arc time of 2000 ms. During the splicing process, the splicer used a cladding alignment method in which the unique core of the SMF and the central core of the SCMCF become precisely aligned. It should be pointed out that the SMF–SCMCF junctions have been demonstrated to have high tensile strength. They withstand more than 3000 microstrains, which ensures that the proposed sensor has enough tensile strength, even in demanding sensing applications [14].

The proposed curvature sensor composes a piece of the SCMCF of 13 mm in length with 2 mm long Bragg gratings written in all the cores of the SCMCF. The experimentally measured reflection spectrum of the fabricated sensor is shown in Fig. 2. It is worth noting that the sensor features two distinct resonance peaks, along with a deep notch between them. The underlying principle of this phenomenon can be explained as follows. Due to the axial symmetry of the SMF–SCMCF structure and the symmetry of the SCMCF, only two supermodes are excited by the fundamental mode of the input SMF under the center-core excitation condition [14]. Here two supermodes are labeled as SM1 and SM2; their 2D profiles are shown in Fig. 3.

The two supermodes propagate together in the SCMCF with different propagation constants. The effective refractive indices of the two supermodes, at 1560 nm and no curvature, were calculated theoretically to be $n_{\text{eff}}^1 = 1.44869$ and $n_{\text{eff}}^2 = 1.44935$ with a commercial simulation software (Lumerical). According

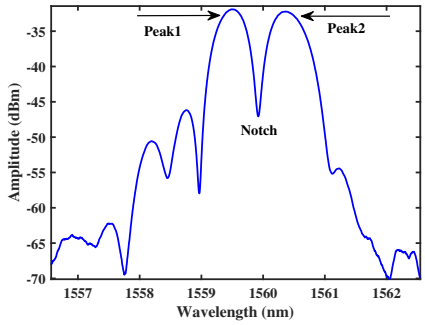

Fig. 2. Measured reflection spectrum of the fabricated sensor.

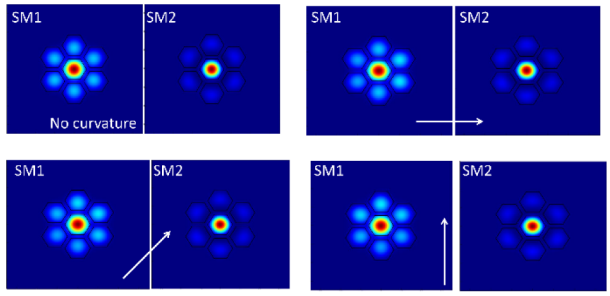

Fig. 3. 2D profiles of the supermodes SM1 and SM2 excited in the SCMCF when no curvature is applied and when the curvature of 1 m^{-1} is applied in the directions indicated with the arrows. In all cases, $\lambda = 1560$ nm.

to the Bragg reflection condition, two reflection peaks can be expected, which are given by the expressions [16]

$$\lambda_{B1} = 2n_{\text{eff}}^1 \Lambda, \tag{1}$$

$$\lambda_{B2} = 2n_{\text{eff}}^2 \Lambda, \tag{2}$$

where Λ is the grating period. In our experiment, the length of the FBG is short (~2 mm), and the refractive index change is relatively weak; thus, the spectrum of an individual FBG has an approximate Gaussian profile. A general expression for the approximate full width at half-maximum bandwidth, $\Delta\lambda_{\text{FWHM}}$, of a grating is given by [17]

$$\Delta\lambda_{\text{FWHM}} = \lambda_{Bs}\sqrt{\left(\frac{\Delta n}{2n_0}\right)^2 + \left(\frac{\Lambda}{L_g}\right)^2}, \tag{3}$$

where L_g is the grating length, Δn is the induced refractive index change, n_0 is the average refractive index, and $s \approx 0.5$ for weak grating. In our previous work, the interferometric sensors using the same SCMCF exhibit an interference pattern with a visibility exceeding 30 dB, which means the two supermodes have almost the same intensity [13]. This is the reason that the two resonance peaks have similar reflectivity. After propagation through a section of the SCMCF, the two reflected signals related to two supermodes are re-coupled into the SMF, and the interference occurs as a result of the phase difference between the two reflection spectra, as shown in Fig. 2. The accumulated phase difference at wavelength λ is $\Delta\Phi = 4\pi\Delta n_{\text{eff}} L_f/\lambda$, where $\Delta n_{\text{eff}} = n_{\text{eff}}^2 - n_{\text{eff}}^1$ and $L_f = 6.5$ mm is the length between the splice junction and the FBG. Consequently, a notch is generated

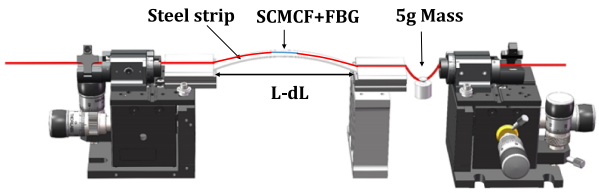

Fig. 4. Experimental setup for the curvature measurement.

in the superposition region between the two adjacent resonance peaks. The depth of the notch will reach maximum values when $\Delta\Phi = m\pi$, where m is an integer.

The experimental setup for curvature sensing is depicted in Fig. 4. To facilitate curvature measurements, both ends of the SCMCF were fusion spliced with the SMF, thus forming an SMF–SCMCF-SMF structure. It should be pointed out that the SCMCF was not recoated, and the coating of the SMF spliced to both sides of the SCMCF was also removed with the length of 4.5 cm. The outer diameters of the SMF and SCMCF are 125 and 140 μm, respectively. A thin steel strip was held at its two ends by a pair of precision translation stages. The sensor was placed on the top of the steel strip, and the FBGs were located in the middle of the steel strip. One of the two translation stages was fixed, while the other one could be moved to or from the fixed stage. Thus, the metal strip could be bent in a controlled manner, and the uniform curvature at the middle section was applied. To ensure that the sensor contacts the steel strip tightly and synchronously bend with the steel strip, a 5 g mass was added to one end to make the fiber structure in a tension state. The relationship between the curvature and displacement of the translation stage can be approximated as

$$\sin\left(\frac{LC}{2}\right) = \frac{(L - dL)C}{2}. \tag{4}$$

In Eq. (4), C is the applied curvature with the units of m^{-1}, and dL is the initial separation and the separation variation, respectively, between two translation stages. In our experiments, L was 125 mm. During the bending process, the environmental temperature was constant, approximately 25°C.

The reflection spectra observed at different curvatures are shown in Fig. 5. It can be noticed that the wavelength positions of the two Bragg resonance peaks show a slight change at different values of curvature. In contrast, the depth of the notch changes drastically when the sensor experiences bending. The notch depth decreases gradually as the curvature increases. The sensing mechanism of our proposed curvature sensor can be explained as follows. Due to the excitation conditions, the central core of the multicore fiber has most of the light intensity; see Fig. 3. Thus, the grating in such a core contributes more to the reflectivity than the gratings written in the surrounding cores. For this reason, there is no obvious shift in the reflected spectrum as the SCMCF is bent. In addition, as the fiber is bent, the effective refractive index difference between two supermodes changes because of the change in the mode profile upon bending. The accumulated phase difference $\Delta\Phi$ between two supermodes involved in the interference is changed and depends on the curvature radius. Thus, the depth of the notch induced by supermode interference is changed. As a result, the bending radius can be found by monitoring the notch depth of the reflection spectrum. Compared to traditional wavelength readout

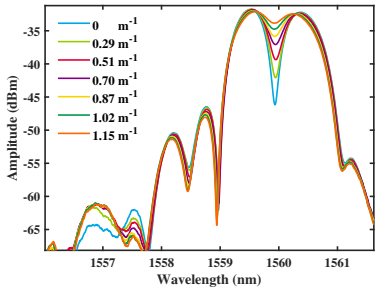

Fig. 5. Spectral response of the sensor at different curvatures.

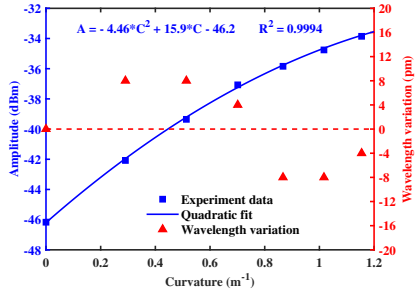

Fig. 6. Amplitude changes and the wavelength variation of the notch as a function of the curvature.

methods, the intensity demodulation method based on the measurement of the notch depth can relax the requirement of OSA's resolution while effectively eliminating the cross-sensitivity problem introduced by temperature.

The relationship between the depth of the notch and curvature is shown in Fig. 6 (blue line). The results indicate that the notch amplitude presents a nonlinear response as a function of the curvature. The expression of the fitting line can be written as

$$A = -4.46C^2 + 15.9C - 46.2, \tag{5}$$

where A is amplitude with the units of decibel-milliwatts. The coefficient of determination (R^2) is 0.9994, indicating that the fitting line is extremely accurate. The device is much more sensitive at low curvature values. The maximum sensitivity was found to be ~15.9 $\mathrm{dB/m^{-1}}$ in the curvature range from 0 to 0.7 $\mathrm{m^{-1}}$. The wavelength variation of the notch as a function of the curvature was also investigated, as shown in Fig. 6 (red triangle). The results show that the wavelength fluctuation is less than 10 pm under the available spectrometer with the resolution of 20 pm, which means the proposed sensor has the potential to be exploited to discriminate other measurands by monitoring wavelength shift such as temperature or strain.

In addition, the response of the device to the curvature in three different bending directions, namely −45°, 0°, and +45° was also analyzed. It must be pointed out that the orientation of the cores is not known experimentally. The initial bending orientation angle ($\theta = 0°$) is set arbitrarily; then the bending angle was changed to analyze the orientation dependent sensitivity. This means that the SCMCF was rotated and then it was subjected to the curvature. The results of our experiments are summarized in Fig. 7. It can be observed that in all cases the changes of the notch amplitude with respect to the curvature have the same trend. The maximum difference in the measured notch amplitude was around 1.1 dB, which is thought

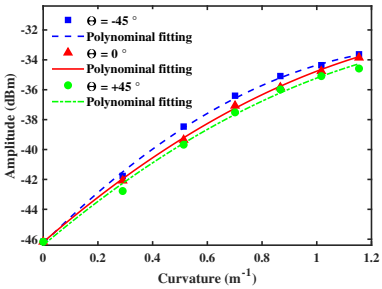

Fig. 7. Amplitude response of the notch against the curvature at different orientations of the SCMCF with respect to the curvature.

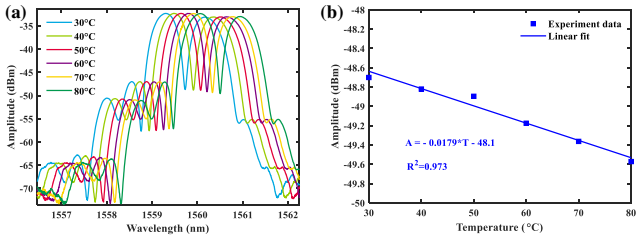

Fig. 8. (a) Spectral response of the sensor at different temperatures. (b) Amplitude variation of the notch under different temperatures.

to be caused by fabrication errors such as the center core not being located on the neutral axis, or the six outer cores not being arranged at the corners of a regular hexagon. The results shown in Fig. 7 suggest that the core orientations of the SCMCF with respect to the applied curvature have a slight effect on the curvature sensitivity.

To further characterize our device as a temperature-insensitive curvature sensor, the temperature dependence of the proposed sensor was also tested. A ceramic tube was used to heat the SCMCF-FBG from 30°C to 80°C with a stability of ±2°C. Each temperature value was maintained for 10 min to guarantee that the sensor was subjected to a stable temperature. Figure 8(a) shows the observed spectra at different temperatures. It can be noted from the figure that the shape of the reflection spectra remains unchanged in the studied temperature range. As expected, the reflection spectrum shifts to the red as temperature increases. The amplitude of the notch as a function of temperature is shown in Fig. 8(b). Note that the notch amplitude decreases linearly as temperature increases. Over the whole testing range, from 30°C to 80°C, the amplitude of the notch changed around 1 dB. The temperature sensitivity that was found when the amplitude of the notch was monitored was −0.0179 dB/°C. As discussed above, the curvature sensitivity of our device is 15.9 dB/m^{-1}. Thus, the cross sensitivity between the curvature and temperature is merely 0.001 m^{-1}/°C, so the impact of temperature on the curvature interrogation can be negligible. Therefore, by intensity demodulation of the notch depth, a temperature-insensitive curvature sensor is achieved.

In conclusion, a novel temperature-insensitive curvature sensor is proposed by combing the SCMCF and FBG. The sensor was fabricated by writing a 2 mm long FBG into an SCMCF first; then it was fusion spliced to the SMF for sensing information interrogation. The FBG written in the SCMCF exhibits unique spectral properties in that the reflection spectrum contains two resonance peaks, along with a deep notch between them. The experiment results show that, by monitoring the notch depth, the proposed sensor can work well as a temperature-insensitive curvature sensor. Compared to weakly coupled MCF-based curvature sensors, the sensing information extraction of our proposed sensor does not require expensive fan-in/out devices, which greatly reduces the complexity and cost of the interrogation system. Although multimode-interference-based curvature sensors have a simpler structure and higher sensitivity compared to our proposed sensor, their multiplexing capability is limited [18,19]. The sensor proposed here has the potential for multi-point measurements, which can be achieved by cascading several sensors with different Bragg wavelengths.

Funding. National Natural Science Foundation of China (62071395); the 111 Project (B18045); Sichuan Province Science and Technology Support Program (2020YJ0329); Universitat Politècnica de València (PAID-01-18); Ministerio de Economía y Competitividad (PGC2018-101997-B-I00, TEC2017-88029-R).

Disclosures. The authors declare no conflicts of interest.

Data Availability. Data underlying the results presented in this paper are not publicly available at this time but may be obtained from the authors upon reasonable request.

REFERENCES

1. X. He, Z. L. Ran, T. T. Yang, Y. Q. Xiao, Y. X. Wang, and Y. J. Rao, Opt. Express **27**, 9665 (2019).
2. C. L. Fu, Y. P. Wang, S. Liu, Z. Y. Bai, J. Tang, L. P. Shao, and X. Y. Liu, Opt. Lett. **44**, 1984 (2019).
3. Y. S. Zhang, Y. X. Zhang, W. G. Zhang, L. Yu, L. X. Kong, T. Y. Yan, and L. Chen, Appl. Opt. **59**, 2352 (2020).
4. S. X. Zhang, Y. Liu, H. Y. Guo, A. Zhou, and L. B. Yuan, IEEE Sens. J. **19**, 2148 (2019).
5. Y. Awaji, J. Sakaguchi, B. J. Puttnam, R. S. Luis, J. M. D. Mendinueta, W. Klaus, and N. Wada, Opt. Fiber Technol. **35**, 100 (2017).
6. I. Gasulla, D. Barrera, J. Hervas, and S. Sales, Sci. Rep. **7**, 41727 (2017).
7. Z. Y. Zhao, Z. Y. Liu, M. Tang, S. N. Fu, L. Wang, N. Guo, C. Jin, H. Y. Tam, and C. Lu, Opt. Express **26**, 29629 (2018).
8. J. P. Moore and M. D. Rogge, Opt. Express **20**, 2967 (2012).
9. D. Zheng, Z. Y. Cai, I. Floris, J. Madrigal, W. Pan, X. H. Zou, and S. Sales, Opt. Lett. **44**, 5570 (2019).
10. Q. Feng, Y. B. Liang, M. Tang, and J. P. Ou, Measurement **164**, 108121 (2020).
11. J. Madrigal, D. Barrera, and S. Sales, J. Lightwave Technol. **37**, 4703 (2019).
12. E. Yamashita, S. Ozeki, and K. Atsuki, J. Lightwave Technol. **3**, 341 (1985).
13. J. E. Antonio-Lopez, Z. S. Eznaveh, P. Likamwa, A. Schülzgen, and R. Amezcua-Correa, Opt. Lett. **39**, 4309 (2014).
14. J. Villatoro, O. Arrizabalaga, G. Durana, I. S. D. Ocáriz, E. Antonio-Lopez, J. Zubia, A. Schülzgen, and R. Amezcua-Correa, Sci. Rep. **7**, 4451 (2017).
15. J. Amorebieta, A. Ortega-Gomez, G. Durana, R. Fernandez, E. Antonio-Lopez, A. Schülzgen, J. Zubia, R. Amezcua-Correa, and J. Villatoro, Sci. Rep. **11**, 5989 (2021).
16. T. Mizunami, T. V. Djambova, T. Niiho, and S. Gupta, J. Lightwave Technol. **18**, 230 (2000).
17. P. St.J. Russell, J. L. Archambault, and L. Reekie, Phys. World **6**, 41 (1993).
18. Y. Gong, T. Zhao, Y. J. Rao, and Y. Wu, IEEE Photonics Technol. Lett. **23**, 679 (2011).
19. S. Silva, E. G. P. Pachon, M. A. R. Franco, P. Jorge, J. L. Santos, F. X. Malcata, C. M. B. Cordeiro, and O. Frazão, J. Lightwave Technol. **30**, 3569 (2012).